

A&A manuscript no.  
(will be inserted by hand later)

Your thesaurus codes are:  
3; (09.10.1; 11.09.1 NGC 253; 11.19.2; 11.19.3; 13.25.2)

ASTRONOMY  
AND  
ASTROPHYSICS

September 30, 2000

# XMM-Newton observations of NGC 253: Resolving the emission components in the disk and nuclear area<sup>\*</sup>

W. Pietsch<sup>1</sup>, K.N. Borozdin<sup>2</sup>, G. Branduardi-Raymont<sup>3</sup>, M. Cappi<sup>4</sup>, M. Ehle<sup>5</sup>, P. Ferrando<sup>6</sup>, M.J. Freyberg<sup>1</sup>, S.M. Kahn<sup>7</sup>, T.J. Ponman<sup>8</sup>, A. Ptak<sup>9</sup>, A.M. Read<sup>1</sup>, T.P. Roberts<sup>10</sup>, M. Sako<sup>7</sup>, R.E. Shirey<sup>11</sup>, and M. Ward<sup>10</sup>

<sup>1</sup> Max Planck Institut für extraterrestrische Physik, Giessenbachstraße, D-85741 Garching bei München, Germany

<sup>2</sup> NIS-2, Space and Remote Sensing Sciences, MS D436 Los Alamos National Laboratory, Los Alamos, NM 87545, USA

<sup>3</sup> Mullard Space Science Laboratory, University College London, Holmbury St. Mary, Dorking, Surrey, RH5 6NT, UK

<sup>4</sup> Istituto TeSRE/CNR, Via Gobetti 101, 40129 Bologna, Italy

<sup>5</sup> XMM-Newton SOC, Villafranca, Apartado 50727, E-28080 Madrid, Spain

<sup>6</sup> DAPNIA / Service d'Astrophysique, Bat. 709 Orme des Merisiers, CEA Saclay, 91191 Gif-sur-Yvette, Cedex, France

<sup>7</sup> Columbia Astrophysics Lab. and Dep. of Physics, Columbia University, 550 W. 120th Street, New York, NY 10027, USA

<sup>8</sup> School of Physics & Astronomy, University Birmingham, Birmingham B15 2TT, UK

<sup>9</sup> Department of Physics, Carnegie Mellon University, USA

<sup>10</sup> Department of Physics & Astronomy, University of Leicester, Leicester LE1 7RH, UK

<sup>11</sup> Department of Physics, University of California, Santa Barbara, CA 93106, USA

Received date; accepted date

**Abstract.** We describe the first XMM-Newton observations of the starburst galaxy NGC 253. As known from previous X-ray observations, NGC 253 shows a mixture of extended (disk and halo) and point-source emission. The high XMM-Newton throughput allows for the first time a detailed investigation of the spatial, spectral and variability properties of these components simultaneously. We detect a bright X-ray transient  $\sim 70''$  SSW of the nucleus and show the spectrum and light curve of the brightest point source ( $\sim 30''$  S of the nucleus, most likely a black-hole X-ray binary, BHXRb). The unprecedented combination of RGS and EPIC also sheds new light on the emission of the complex nuclear region, the X-ray plume and the disk diffuse emission. In particular, EPIC images reveal that the limb-brightening of the plume is mostly seen in higher ionization emission lines, while in the lower ionization lines, and below 0.5 keV, the plume is more homogeneously structured, pointing to new interpretations as to the make up of the starburst-driven outflow. Assuming that type IIa supernova remnants (SNRs) are mostly responsible for the  $E > 4$  keV emission, the detection with EPIC of the 6.7 keV line allows us to estimate a supernova rate within the nuclear starburst of  $0.2 \text{ yr}^{-1}$ .

**Key words:** X-rays: galaxies – Galaxies: individual: NGC 253 – Galaxies: spiral – Galaxies: starburst – Interstellar medium: jets and outflows

Send offprint requests to: W. Pietsch (wnp@mpe.mpg.de)

<sup>\*</sup> Based on observations with XMM-Newton, an ESA Science Mission with instruments and contributions directly funded by ESA Member States and the USA (NASA).

## 1. Introduction

X-ray emission from starburst galaxies is known to be complex, revealing both point sources and diffuse X-ray emission in abundance. X-ray binaries, supernovae, supernova remnants and nuclear sources dominate the point-like source contribution, while the hot phases of the interstellar medium (ISM), in the form of hot outflows (or winds), more bound coronal features and diffuse emission within the disk, make up the diffuse, gaseous component.

The nearby edge-on galaxy NGC 253 is perhaps the classic example (along with M82) of a starburst galaxy, and as such, has received a great deal of attention from X-ray observatories over the years. Initial *Einstein* observations (Fabbiano & Trinchieri 1984, Fabbiano 1988), along with seeing several bright point-like disk sources, discovered large plumes of diffuse emission extending above and below the disk of the galaxy. Though originally thought to be due to  $10^6$  K gaseous clouds, ejected from the starburst nucleus, it was later thought that this emission could be due to supernovae and winds from massive stars in the central starburst driving a large-scale outflow that shock heats and accelerates ambient interstellar and circumnuclear gas in the form of a galactic wind (Heckman et al. 1990).

Several studies were made of NGC 253 with ROSAT. Both the PSPC and HRI data were presented by Read et al. (1997) and Dahlem et al. (1998). An extensive ROSAT point source catalogue of NGC 253 by Vogler & Pietsch (1999), made it possible to separate the point source and

diffuse X-ray emission, allowing insights into the spatial, spectral and timing properties of the many point sources within NGC 253. The ‘nuclear’, likely starburst-associated source appeared to be extended, and the brightest point-like source, lying some  $30''$  south of the nucleus, at the border of a plume of diffuse emission, was thought to be a plausible BHXRB candidate. Structure in the diffuse emission could now be studied in detail, Pietsch et al. (2000) reporting different diffuse emission components in the nucleus, disk and halo. Especially of note was the discovery of coronal diffuse emission bubbling out of the disk, via galactic *fountains* and *chimneys* (essentially formed by localized high-activity star-forming regions within the disk), then falling ballistically back to the plane (e.g. Norman & Ikeuchi 1989). Also observed was a hollow-cone shaped diffuse plume of emission extending up to  $\sim 700$  pc along the SE minor axis, thought to be due to the interaction of the galactic superwind and the dense disk ISM.

More recent high spectral resolution observations with ASCA (Ptak et al. 1997) have revealed strong O, Ne, Fe, Mg, S and Si emission lines in the integrated NGC 253 spectrum, and these results have been backed up by BeppoSAX observations (Cappi et al. 1999), where for the first time, the 6.7 keV Fe K line has been detected (Persic et al. 1998). *Chandra* observations allowed for the first time a detailed study of the SE plume, tentatively observed with ROSAT, to be a well-collimated, limb-brightened kpc-scale conical outflow, which closely follows in morphology the known H $\alpha$  outflow. Furthermore, several point sources are seen, the nuclear feature being partly separated into a number of distinct sources (Strickland et al. 2000).

In this letter we report the results of the performance verification phase observation of NGC 253 to demonstrate XMM-Newton’s capabilities of spatially resolved spectroscopy in a mixture of point sources and diffuse emission.

## 2. Observations and data analysis

NGC 253 was observed with the European X-ray observatory XMM-Newton (Jansen et al. 2001) during orbit 89 on 2000 July 3rd and 4th for two exposures each of the European Photon Imaging Camera instruments (EPIC, Turner et al. 2001, Strüder et al. 2001) and the Reflection Grating Spectrometer (RGS, den Herder et al. 2001). For details of the instrument setups and exposure durations for the different instruments see Table 1. The position angle of the observation ( $55^\circ$ ) was close to the position angle of the galaxy ( $52^\circ$ ), and so, to minimize the effect of the EPIC PN CCD boundaries on the plume and disk emission, the nominal on-axis pointing position was offset by  $65''$  to the SE of the NGC 253 nucleus along the galaxy’s minor axis.

The standard reduction of the EPIC and RGS data was performed using the Science Analysis System (SAS). This involved the subtraction of hot, dead or flickering pixels, removal of events due to electronic noise and, for the EPIC detectors, correction of event energies for charge transfer

**Table 1.** Details of NGC 253 XMM-Newton exposures. Exposure number (E), instrument setting and exposure duration and low background time (LB) are given.

| E | Det. | Filter | Mode       | Dur.<br>(s) | LB<br>(s) |
|---|------|--------|------------|-------------|-----------|
| 1 | RGS1 |        | SPECTR + Q | 60 613      | 47 313    |
|   | RGS2 |        | SPECTR + Q | 60 593      | 47 293    |
|   | MOS1 | Medium | PRI FULL   | 38 498      | 34 492    |
|   | MOS2 | Thin   | PRI FULL   | 38 498      | 34 489    |
|   | PN   | Medium | PRI FULL   | 39 000      | 35 767    |
| 2 | RGS1 |        | SPECTR + Q | 17 402      | 6 102     |
|   | RGS2 |        | SPECTR + Q | 17 406      | 6 106     |
|   | MOS1 | Medium | PRI FULL   | 13 593      | 7 190     |
|   | MOS2 | Thin   | PRI FULL   | 13 597      | 7 188     |
|   | PN   | Thin   | PRI FULL   | 13 999      | 7 400     |

losses. Also, times of high background were excluded to maximize sensitivity to low surface brightness emission. While exposure 1 was interrupted by just a short background flare, a major part of exposure 2 suffered from high background (see duration of low background (LB) per exposure in Table 1). Source searching was performed on the cleaned MOS1, MOS2 and PN datasets separately. After comparing these source lists, the MOS datasets were transformed to the PN positions, whereupon, merging of the cleaned, aligned EPIC datasets took place. A final transformation of the EPIC merged dataset to ROSAT positions was then performed.

For the RGS, source events from the total observation were first extracted using a  $1'$  spatial mask in the cross-dispersion direction (i.e. along the minor axis centered on the bright nuclear area), and subsequently with a dispersion/pulse-height mask to select the first-order photons. The background spectrum was estimated using the same observation from regions  $> 1'$  from the nucleus, which may contain events from the galaxy’s diffuse emission. Data from the two RGS’s are combined and divided by the exposure and the effective area of the instrument.

## 3. X-ray emission from the disk

The EPIC data clearly reveal more point sources than the deep ROSAT observations and allow the mapping of diffuse emission in the disk (Fig. 1). In the following we concentrate on the ten brightest NGC 253 sources and present a brief analysis of the diffuse emission in the disk.

### 3.1. Point sources

We searched for the ten brightest on-galaxy sources detected with the highest maximum likelihood in the summed low background MOS 1 and MOS 2 images to find new NGC 253 X-ray transients (Table 2). Where available we use the source numbers introduced for the ROSAT

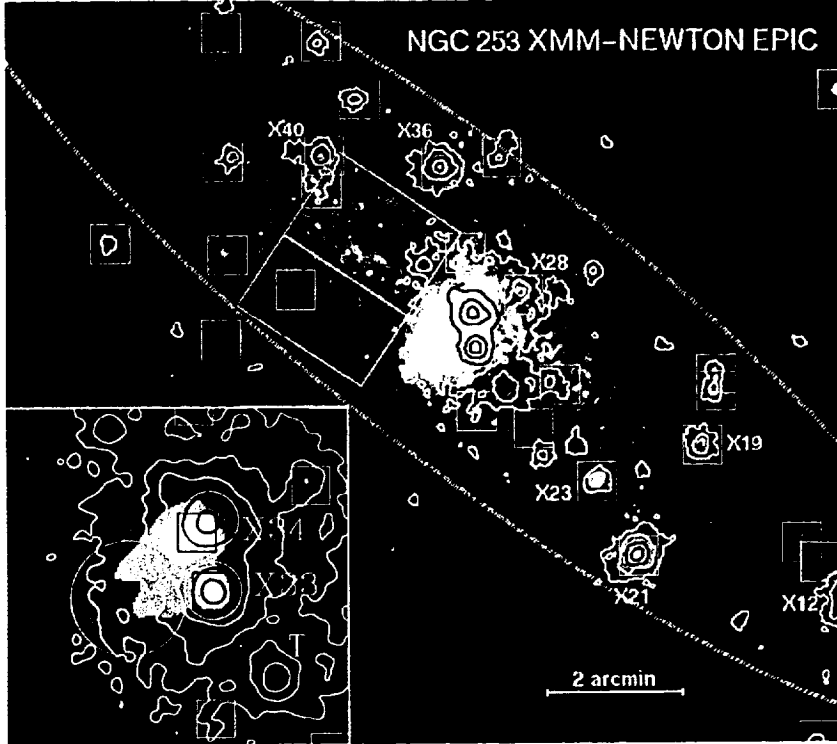


**Fig. 1.** Logarithmically-scaled, three-colour XMM-Newton EPIC image of the NGC 253 disk and nuclear regions. Emission detected in all three EPIC instruments (MOS1, MOS2 and PN) has been separately cleaned and merged together. Red, green and blue show respectively the ROSAT-equivalent (0.2–0.5) keV, (0.5–0.9) keV and (0.9–2.0) keV bands, while the hard (2–10 keV) emission is shown superimposed as black/white contours at levels increasing by factors of 3 from  $0.3 \text{ ct arcsec}^{-2}$ . The data in each energy band have been smoothed with a PSF-equivalent Gaussian of FWHM  $5''$ . Shown in detail to the lower left is a higher-threshold factor 2 zoom-in on the nuclear region. Squares indicate the position of ROSAT-detected sources (Vogler & Pietsch 1999), and source identifications referred to in this paper (including the newly discovered transient, T) are marked. Spectral extraction regions (white rectangles and, in inset, yellow circles) and the inclination-corrected optical  $D_{25}$  ellipse of NGC 253 are marked

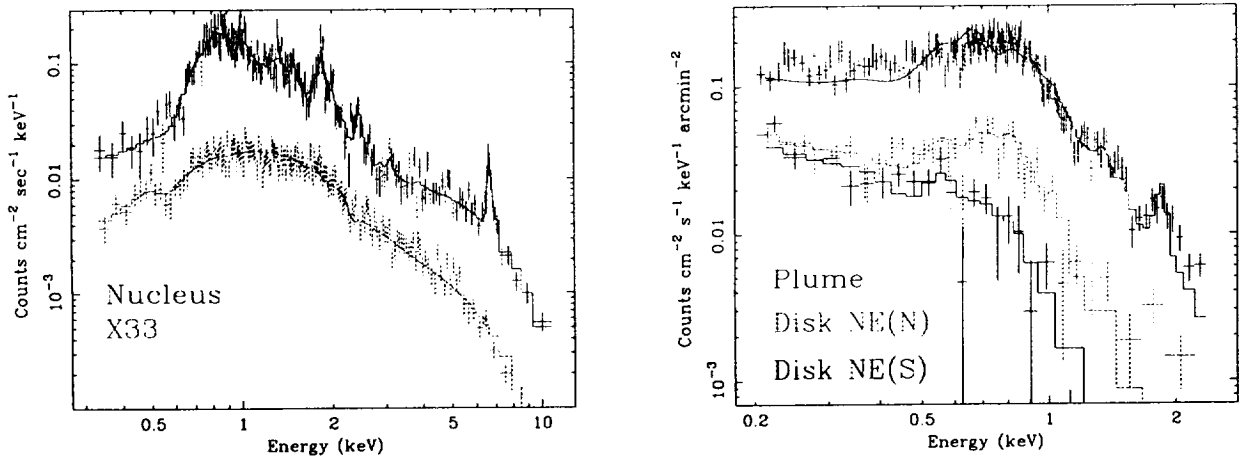


**Fig. 2.** EPIC PN background subtracted spectra from low background times of the first exposure with spectral models (see text) indicated. **Left:** Spectra of extended nucleus and X33 (extraction radius  $12''.5$ , local background subtracted, X33 intensity shifted down by 0.5 decade for clarity). **Right:** spectra of SE X-ray plume and two areas of the disk NE of the nucleus (0.5, 2.5, and  $2.4 \text{ arcmin}^2$  extraction regions, respectively [see Fig.1], point sources removed, background from absorbed region NE of X36)

NGC 253 point-like sources (Vogler & Pietsch 1999). This list was confirmed by a visual inspection, and source X28 was added (detected by PN only, though obviously real). For two sources (X21 and X40) PN count rates are not given as they lie close to the chip gaps. The apparently separate sources X17/X18 could not be distinguished by

the detection algorithms, and hence will be discussed in a later full point source analysis of NGC 253.

Count rates were calculated using the total source count output in the 0.2–10 keV band from the SAS source detection software. Due to the complex background, the 4 sources closest to the nucleus (X34, X33, X28 and T) were treated individually. We assumed a systematic error

**Table 2.** Bright point-like sources within NGC 253: EPIC (MOS1+2 & PN) count rates, hardness ratios (with errors on the last digit[s]) and luminosities in  $10^{37}$  erg s $^{-1}$  both for EPIC (B) broad (0.2–10 keV) band and for comparison (S) ROSAT (0.2–2.4 keV) band (assumed NGC 253 distance: 2.58 Mpc).

| Src. | Count rate        |         | EPIC hardness ratios |          |          | $L_x^B$       | $L_x^S$       |
|------|-------------------|---------|----------------------|----------|----------|---------------|---------------|
|      | MOS1+2            | PN      | HR1                  | HR2      | HR3      |               |               |
|      | (cts ks $^{-1}$ ) |         |                      |          |          | ( $10^{37}$ ) | ( $10^{37}$ ) |
| X34  | 445(23)           | 470(24) | 1.00(0)              | -0.49(1) | -0.40(1) | 120           | 49            |
| X33  | 303(15)           | 293(15) | 1.00(0)              | -0.12(1) | -0.57(1) | 95            | 32            |
| X21  | 169( 4)           |         | 0.85(1)              | -0.40(1) | -0.66(2) | 50            | 20            |
| X36  | 86( 2)            | 111( 3) | 0.94(1)              | -0.39(1) | -0.75(2) | 23            | 9.5           |
| X12  | 81( 2)            | 99( 3)  | 0.97(1)              | -0.16(2) | -0.67(2) | 25            | 7.5           |
| T    | 28( 2)            | 26( 2)  | 0.88(2)              | -0.10(3) | -0.33(3) | 14            | 2.1           |
| X40  | 27( 1)            |         | 0.89(3)              | -0.25(3) | -0.45(4) | 9.2           | 2.8           |
| X19  | 19( 1)            | 26( 1)  | 0.80(3)              | -0.41(3) | -0.46(5) | 5.5           | 1.8           |
| X28  | 17( 1)            | 24( 1)  | 0.86(2)              | -0.54(2) | -0.61(5) | 4.7           | 1.5           |
| X23  | 17( 1)            | 22( 1)  | 0.53(3)              | -0.57(3) | -0.47(7) | 4.6           | 2.3           |

for the count rates of 5% for the 4 near-nuclear sources and 2% for the other sources which dominates the overall error. Hardness ratios (HRs) were determined from 4 bands (0.2–0.5 keV, 0.5–2.0 keV, 2.0–4.5 keV, 4.5–10.0 keV) by aperture photometry to get raw counts per source per band on combined low background images from all the detectors and exposures. The HRs have been calculated as hard – soft / hard + soft, with HR1 being 0.2–0.5 keV vs 0.5–2 keV and so on ('soft' here means the count rate in the 0.2 – 0.5 keV band etc.) with errors as per Appendix A of Ciliegi et al. 1997.

All bright persistent sources known from the ROSAT observations are also detected by XMM-Newton. While the EPIC luminosity of most of the sources is similar to that measured by ROSAT, X21 is brighter by a factor of 2 and X40 fainter by more than a factor of 3. In addition we detect  $\sim 70''$  SSW of the nucleus one new bright transient source (T,  $\alpha_{2000} = 0^h 47^m 30^s.9$ ,  $\delta_{2000} = -25^\circ 18' 26''$ ) that already was visible during the *Chandra* observation half a year earlier (Strickland et al. 2000). HR1 is a good indicator of the absorption depth within NGC 253 under which a source is seen, while HR2 and HR3 characterize the spectrum. T is clearly the hardest source in the sample. X33, X12, and X40 show similarly hard spectra. Together with the X-ray luminosity this may indicate that these sources are BHXRBS and the transient may be an X-ray nova such as have been seen in our Galaxy. X21, X36, X19, X28, and X23 have softer spectra, indicative of low mass X-ray binaries (LMXB) or SNRs. Most of the sources show time variability during the ROSAT and/or XMM-Newton observations, arguing for a LMXB nature. The low ROSAT HR2 of X23 and lack of time variability may point to it being a SNR.

While a detailed spectral and time variability study of all the NGC 253 sources is beyond the scope of the

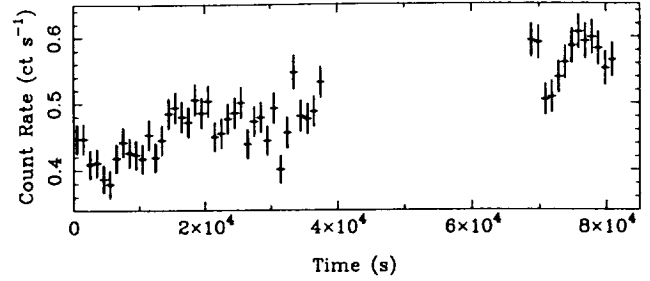


**Fig. 3.** X33 EPIC light curve. Data from all EPIC instruments in the 0.5–10 keV band are integrated over 1000 s bins

present paper, we demonstrate here the capabilities of the EPIC instrument on the brightest point source, X33. Its spectrum (Fig. 2) can be fit by a thermal bremsstrahlung model, assuming an absorbing column of  $N_H = (2.50 \pm 0.17) 10^{21} \text{ cm}^{-2}$  and temperature of  $(5.3 \pm 0.5) \text{ keV}$  ( $\chi^2_{\text{red}} = 0.98$  for 180 d.o.f.). Considering the uncertainty in selecting a local background, the preferred model for BHXRBS is also acceptable (absorbed power law,  $N_H = (3.40 \pm 0.24) 10^{21} \text{ cm}^{-2}$  and photon index of  $1.96 \pm 0.06$ ,  $\chi^2_{\text{red}} = 1.26$  for 180 d.o.f.). X33 (as well as X21) varies by a factor  $\sim 2$  during the XMM-Newton observation (see Fig. 3).

### 3.2. Diffuse disk emission

The EPIC image reveals unresolved emission from the inner disk that is harder along the inner spiral arms. We extracted EPIC PN disk spectra NE of the nucleus, selecting areas of harder emission in the N and softer in the S (yellow greenish and red; see rectangles in Fig. 1). While the spectra below 0.5 keV are very similar (Fig. 2), the NE(N) shows additional emission extending to energies of  $\sim 2 \text{ keV}$  and indications of emission lines pointing to emission from hot gas. While ISM components with several temperatures together with unresolved point sources will most likely contribute to the spectrum, we modeled the spectra with an unabsorbed, cooler and an additional harder, absorbed thin thermal component fixed to solar abundance. While, as expected, the fits are poor, we find for the NE(N)  $kT_1 = (0.12 \pm 0.02) \text{ keV}$ ,  $N_H^{T_2} = 1.80^{+1.7}_{-1.1} 10^{21} \text{ cm}^{-2}$  and  $kT_2 = 0.36^{+0.12}_{-0.08} \text{ keV}$  ( $\chi^2_{\text{red}} = 1.78$  for 34 d.o.f.), and for the NE(S)  $kT_1 = (0.10 \pm 0.03) \text{ keV}$ ,  $N_H^{T_2} < 0.8 10^{21} \text{ cm}^{-2}$  and  $kT_2 = (0.35 \pm 0.2) \text{ keV}$  ( $\chi^2_{\text{red}} = 1.43$  for 18 d.o.f.). These results are consistent with the soft component originating in the halo above the disk and the harder component from hot ISM embedded in the spiral arms.

### 4. Emission from the nuclear region

The nuclear region of NGC 253 (see inlay Fig. 1) is bright enough for a detailed study with both RGS and EPIC. The RGS spectrum (Fig. 4) is dominated by emission lines of hydrogenic and heliumlike charge states of the abundant low Z elements (N, O, Ne, Mg, Si) and the neonlike and

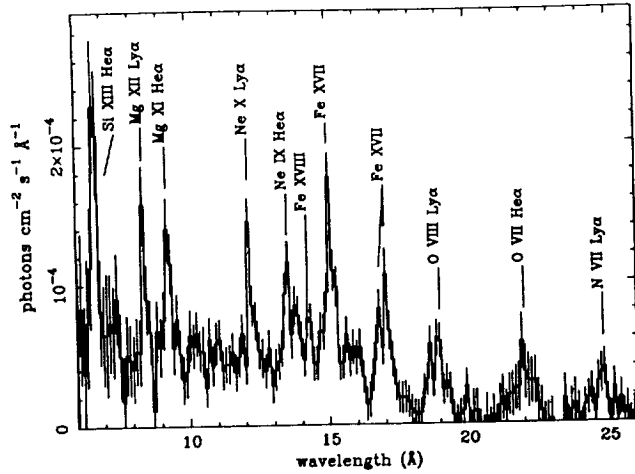


Fig. 4. “Fluxed” RGS spectrum of the bright nuclear area of NGC 253 (extraction region 1’ along the minor disk axis, covering nucleus and plume). Bright emission lines are identified

fluorinelike charge states of Fe. With the help of EPIC we can further localize the RGS emission components in the nuclear area (e.g. Fig. 6). We have not performed quantitative spectral fits to the RGS data, but several conclusions can be drawn directly from the Fig. 4. In general, the spectrum indicates emission from a collisional plasma with a range of temperatures stretching from  $\sim 300$  eV (O VII, Fe XVII) to  $\sim 1.5$  keV (Mg XII, Si XIII). The weakness of the longer wavelength lines suggests significant photoelectric absorption with implied column densities in the range  $10^{21}$ – $10^{22}$   $\text{cm}^{-2}$ . The abundances do not appear to be unusual, although accurate abundance estimates will depend on the precise temperature distribution, which has yet to be determined. The general appearance of the spectrum is reminiscent of the spectrum of intermediate age supernova remnant gas, as might be expected for a starburst nucleus and the interaction of the outflowing wind with the cooler gas of the ISM in the plume. The characteristic emission measure in this region is  $\sim 7.5 \cdot 10^{61}$   $\text{cm}^{-3}$  (assuming solar abundances), which, given the  $30''$  extent of the nuclear source, implies a characteristic electron density of  $\sim 0.1$   $\text{cm}^{-3}$ .

#### 4.1. Unresolved X-ray nucleus

Below 0.5 keV, no significant emission from the unresolved nuclear source (X34) can be seen. As we go to higher energies, the centroid of the X34 emission shifts to the NW along the minor axis (Fig. 5) towards the position of the radio nucleus indicating that only at energies above 4 keV will emission from the nuclear starburst dominate the X-ray spectrum. It is apparent also in the inlay of Fig. 1, that harder (bluer) emission is shifted more to the NW where the black contours of the (2–10) keV emission are centered on the radio nucleus. The natural explanation is that X34

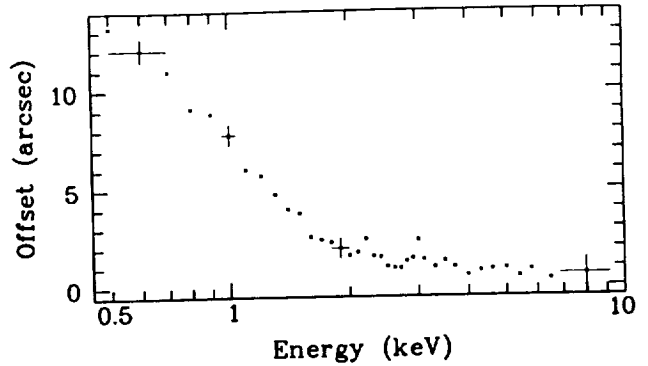


Fig. 5. Distance of the center of the X-ray emission from the position of the galaxy nucleus as a function of energy. The position in RA and Dec has been determined using at least 500 photons per energy bin in a radius of  $12''.5$ . There is a strong shift along the minor axis of  $10''$  from 0.5 to 1.5 keV and a smaller shift up to 4 keV. Typical errors are indicated

is an unresolved source of similar size to the shift reaching out from the starburst nucleus (i.e. the collection of sources and diffuse emission as seen with *Chandra*), that is increasingly absorbed towards the galaxy centre in the intervening inner disk of NGC 253.

The EPIC spectrum further characterizes the nuclear emission (Fig. 2). While the resolution is not sufficient to resolve the lines seen by the RGS below 1 keV, lines from Mg XI, Mg XII, Si XIII, Si XIV, Ar XVI, and Fe XXV are clearly detected and argue for gas components with temperatures up to 5 keV and above. We modeled the spectrum using thin thermal plasma components of solar abundance with corresponding absorption increasing with the temperature of the plasma component and added a power law component with the lowest absorption value. A model with three temperature components gave an acceptable fit ( $\chi^2_{\text{red}} = 1.05$  for 222 d.o.f.) with  $N_{\text{H}} = (0.34, 1.78, 13.2) \cdot 10^{22}$   $\text{cm}^{-2}$ , photon index of 1.0, and temperatures of (0.56, 0.92, 6.3) keV, respectively. A model with the same abundance in all three temperature components does not require the power law component and gives for an abundance of 0.7 solar an equally acceptable fit with very similar absorption values and temperatures. Note that within the nuclear spectrum, no evidence for a significant AGN contribution is detected and the very hard component will originate purely from the starburst nucleus. The column density of  $> 10^{23}$   $\text{cm}^{-2}$  is in good agreement with the predictions from other wavelengths (see discussion in Pietsch et al. 2000).

The energy, intensity and equivalent width of the FeK line are  $(6.67 \pm 0.05)$  keV,  $(7 \pm 2) \times 10^{-7}$  photons  $\text{cm}^{-2} \text{s}^{-1}$  and  $(930 \pm 300)$  eV. Similar high-temperature plasma and FeK lines have been found by XMM-Newton in young type Ib and type IIa SNRs, such as Cas A (age 300 yr) and N 132D (3000 yr) (e.g. Behar et al. 2001). Assuming that type IIa SNRs are prevalent within the starburst nucleus of NGC 253, and assuming the Behar et al. Fe line flux ob-